

# Impact damping and vibration attenuation in nematic liquid crystal elastomers

Mohand O. Saed<sup>1,2</sup>, Waiel Elmadih<sup>3</sup>, Andrew Terentjev<sup>2</sup>, Dimitrios Chronopoulos<sup>4\*</sup>, David Williamson<sup>1</sup>, Eugene M. Terentjev<sup>1\*</sup>

<sup>1</sup> Cavendish Laboratory, University of Cambridge, J.J. Thomson Avenue, Cambridge, CB3 0HE, U.K.

<sup>2</sup> Cambridge Smart Plastics Ltd., 18 Hurrell Rd, Cambridge CB4 3RH, U.K.

<sup>3</sup> Institute for Aerospace Technology, University of Nottingham, Nottingham NG7 2RD, U.K.

<sup>4</sup> Department of Mechanical Engineering (LMSD), KU Leuven, Ghent Technology Campus, 9000, Belgium

E-mail: dimitrios.chronopoulos@kuleuven.be, emt1000@cam.ac.uk

## Abstract

Nematic liquid crystal elastomers (LCE) exhibit unique mechanical properties, placing them in a category distinct from other viscoelastic systems. One of their most celebrated properties is the ‘soft elasticity’, leading to a wide plateau of low, nearly-constant stress upon stretching, a characteristically slow stress relaxation, enhanced surface adhesion, and other remarkable effects. The dynamic soft response of LCE to shear deformations leads to the extremely large loss behaviour with the loss factor  $\tan\delta$  approaching unity over a wide temperature and frequency ranges, with clear implications for damping applications. Here we investigate this effect of anomalous damping, optimising the impact and vibration geometries to reach the greatest benefits in vibration isolation and impact damping by accessing internal shear deformation modes. We compare impact energy dissipation in shaped samples and projectiles, with elastic wave transmission and resonance, finding a good correlation between the results of such diverse tests. By comparing with ordinary elastomers used for industrial damping, we demonstrate that the nematic LCE is an exceptional damping material and propose directions that should be explored for further improvements in practical damping applications.

**Keywords:** liquid crystal elastomer, vibration damping, impact damping, acoustic attenuation.

### 33 **Introduction**

34 There is an increasing interest in new materials that can efficiently dissipate mechanical energy,  
35 both from a fundamental understanding of viscoelasticity and practically in the area of  
36 suppressing vibration and protecting from impact. Examples of applications with high demand  
37 in damping include the automotive, aerospace, wind energy and home appliance industries, but  
38 in reality, the list is much wider. The damping of vibration energy arises due to the energy loss  
39 processes in a viscoelastic material that convert the vibrational energy into heat in either free  
40 or constrained layer configurations.<sup>1,2</sup> The characteristics of the damping material are reflected  
41 in the linear complex modulus  $E^*(f)$  at a given oscillation frequency  $f$ , characterised by its real  
42 and imaginary parts: the storage and loss moduli  $E'$  and  $E''$ , and their ratio  $E''/E'$ , usually  
43 referred to as the loss factor  $\tan\delta$  with  $\delta$  the phase angle of  $E^*$ .<sup>3</sup> The loss factor  $\tan\delta$  is directly  
44 related to the other parameters describing damping:  $\tan\delta = 2\zeta = 1/Q$ , where the ‘quality factor’  
45  $Q$  and the ‘damping ratio’  $\zeta$  are commonly used in the analysis of resonance circuits and  
46 engineering constructions. In mechanical engineering, it is known that merely by assembling a  
47 metal construction with joints and fasteners, already produces a resonance damping with  $Q < 100$   
48 ( $\tan\delta > 0.01$ ), so a substantial increase above this is desired. In addition, for optimal damping,  
49 it is desirable to have a high loss factor over a wide temperature and frequency ranges. With  
50 most current polymeric materials for damping, the properties are optimised only for particular  
51 values of temperature and frequency, often corresponding to their glass transition, where the  
52  $\tan\delta$  has a large peak.<sup>2,4</sup> The ideal materials must also have other attributes to be effective in  
53 practical situations, such as thermal stability, ease of forming complex shapes, good adhesion,  
54 possibility for large-scale manufacture, and ease of application.

55

56 Liquid crystalline elastomers (LCEs) are amorphous rubbers with spontaneous orientational  
57 order of their anisotropic molecular segments. They possess the combination of physical

58 properties that place them in a separate category from any other elastic or viscous material.<sup>5</sup>  
59 The nature of this uniqueness lies in coupling of rubber elasticity and liquid crystalline degrees  
60 of freedom in the elastomer matrix. In ordinary elastic solids, the deformations are created by  
61 the relative movement of the same atoms (or molecules) that form the bonded low-symmetry  
62 lattice. Hence, when the deformation is small, the lattice symmetry is preserved, and one obtains  
63 an ordinary elastic response (although sometimes anisotropic); large deformations destroy the  
64 lattice integrity and break the material. In elastomers and gels, the macroscopic elastic response  
65 arises from the entropy change of polymer chains on stretching their crosslinked end points,  
66 which are far apart. What happens to chain segments on a smaller length scale is a matter  
67 relatively independent of what defines rubber elasticity. For instance, when the orientational  
68 nematic order is established within network strands, its director could rotate independently from  
69 the deformation of crosslinking points. Such an internal orientational degree of freedom within,  
70 and coupled to the elastic body, constitutes what is known as the Cosserat medium,<sup>5,6</sup> an  
71 example of an elastic medium with a mobile internal microstructure.<sup>7</sup> However, the LCEs are  
72 even richer than a nominal Cosserat solid since rubbers are capable of large shear deformations,  
73 being at the same time essentially incompressible. Hence, one expects, and indeed finds, a  
74 variety of unique mechanical properties described in some detail in the defining book on the  
75 subject.<sup>5</sup>

76  
77 The striking feature of LCE having been well studied in the equilibrium regime is the ‘soft  
78 elasticity’, which manifests as a wide, almost zero-stiffness plateau of low nearly-constant  
79 stress upon increasing strain, and is caused by internal rotation of the local director axis, which  
80 absorbs the applied strain without an elastic energy cost.<sup>8,9,10</sup> The interest in ‘dynamic soft  
81 elasticity’ of nematic LCEs<sup>11,12,13,14</sup> has been driven by the unusual aspects of the dynamic-  
82 mechanical response, and in particular, the unusual properties of elastic waves propagating in  
83 LCE.<sup>15,16</sup> One of the key features is the anomalous mechanical damping, increasing with the

84 increased vibration frequency.<sup>16</sup> Notably, only the nematic phase of LCE was proven attractive  
85 for vibration damping: in smectic LCEs,<sup>17</sup> the coupling between crosslinks and the layer  
86 positions leads to strong internal constraints resulting in the pronounced hysteretic shape-  
87 memory effects.<sup>18,19</sup>

88  
89 Here we study and compare the impact damping and vibration attenuation of nematic LCE  
90 materials, optimising the geometry of impact or vibration deformation to maximize the internal  
91 shear component that initiates the anomalous LCE dissipation. We also optimise the choice of  
92 the nematic LCE, taking into account the required energy damping maximisation and the  
93 practicalities of industrial material production. We also compare a range of LCE against current  
94 market-leading damping materials, using different testing methods for impact absorption and  
95 vibration (elastic) attenuation.

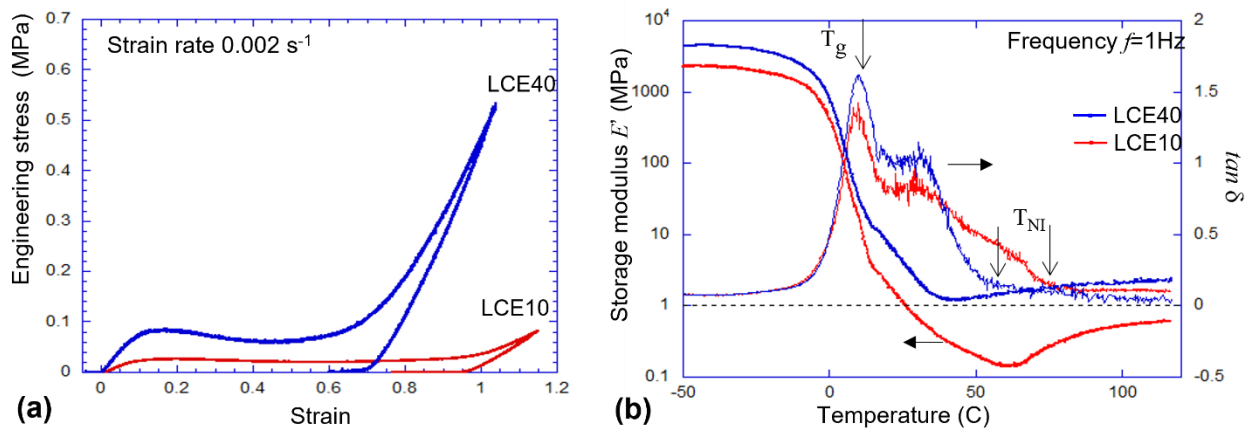
96

## 97 **Results**

### 98 Characterisation of LCE materials

99 The best current LCE materials are based on the robust and error-proof ‘click’ chemistry of  
100 thiol-acrylate Michael addition,<sup>20</sup> using the cheap commercially available starting materials and  
101 easily controlled crosslinking density ([Supplementary Fig.S1](#)). For practical applications, we  
102 need naturally non-aligned, polydomain LCEs<sup>21</sup> with relatively low crosslinking density,  
103 which show the wide stress plateau reflecting the elastic softness on nematic director alignment,  
104 see [Figure 1a](#), comparing the basic LCEs with two crosslinking densities: 10% and 40% (as  
105 labelled in the plot). [Figure 1b](#) shows the typical oscillating dynamic-mechanical response of  
106 an LCE, scanning the temperature range at a fixed frequency, again comparing the crosslinking  
107 densities in the same materials labelled LCE10 and LCE40, respectively. The result illustrates  
108 the key regimes of the dynamic response: the rigid low-dissipation glass below a glass transition  
109  $T_g$ , the low-modulus high-damping nematic range below the nematic-isotropic transition  $T_{NI}$ ,

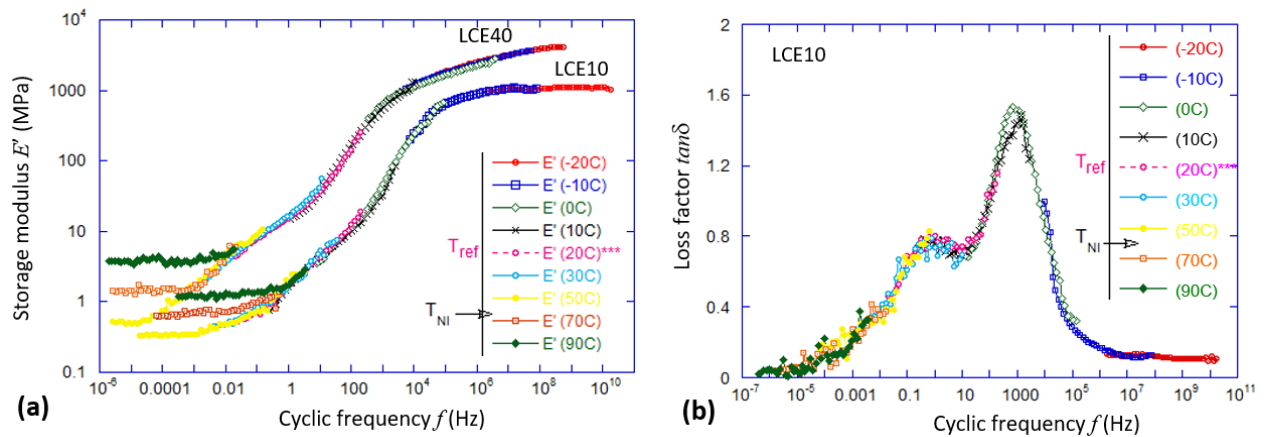
110 and the ordinary isotropic rubber above  $T_{NI}$ . The anomalous damping window between the glass  
 111 at low temperature and the isotropic phase at high temperature is roughly [5-60°C] in these  
 112 LCEs. There is a large literature on how one can control both these key transitions by chemical  
 113 modifications, moving the transition temperatures up or down (see the discussion in  
 114 [Supplementary](#)); this was not our focus in this study. While the test in [Fig. 1b](#) shows the  
 115 components of complex tensile modulus  $E^*(\omega, T)$ , the theory of LCE response<sup>11,12</sup> makes it  
 116 clear that only the shear deformation carries the anomalous dynamic soft elasticity; not  
 117 surprisingly, the early published data showed much higher  $\tan\delta$  values, being tested in the pure  
 118 shear geometry.<sup>10,14</sup>



119 **Fig. 1. Mechanical characterisation of LCE materials.** (a) Near-equilibrium stress-strain  
 120 curves for LCE10 and LCE40 materials, highlighting the wide soft plateau through internal re-  
 121 orientation of the polydomain LCE on stretching, as well as the ability to withstand large  
 122 deformations. (b) Temperature scan of linear oscillating response (at fixed 1Hz), highlighting  
 123 the high  $\tan\delta$  across all of the nematic range.  
 124

125  
 126 [Figure 2a](#) presents the Master Curves of frequency dependence of the linear dynamic modulus  
 127 (tensile modulus, as in [Fig. 1b](#)). Note that above the glass transition one has  $E \approx 3G$ , given the  
 128 effective incompressibility of rubbers and the average isotropy of polydomain LCE, with the  
 129 bulk modulus remaining high:  $K > 2\text{GPa}$ . These Master Curves have the frequency scaled by  
 130 time-temperature superposition,<sup>11,12</sup> using the  $T=20^\circ\text{C}$  as the reference temperature; the unusual

131 behaviour of  $E'(\omega)$  at low frequencies reflects the dynamic soft elasticity when the quasi-  
 132 equilibrium modulus in the nematic LCE phase is much lower than in the isotropic phase above  
 133  $T_{NI}$ . Unlike in ordinary polymers, where the Williams-Landel-Ferry (WLF) time-temperature  
 134 superposition<sup>3</sup> is based on the changing timescales during the glass transition, in nematic LCE  
 135 (well below its  $T_g$ ) the rubbery response adds the additional complexity: the lower modulus in  
 136 the nematic phase due to the internal director relaxation modes (the origin of anomalous  
 137 damping), and the increasing rubber modulus in the isotropic phase above  $T_{NI}$  (due to the  
 138 entropic rubber elasticity  $E \sim k_B T$ ). [Supplementary Fig.S2](#) gives more detail on this procedure  
 139 and the building of Master Curves in LCE.



140

141 **Fig. 2. Master Curves of LCE materials.** (a) The tensile storage modulus  $E'(\omega)$  for LCE10  
 142 and LCE40 materials, obtained by time-temperature superposition of frequency-scan tests at  
 143 different temperatures (labelled in the plot) with the frequency scaled for the reference  $T=20^\circ\text{C}$ .  
 144 The nematic transition  $T_{NI}$  for both materials is between 50 and  $70^\circ\text{C}$  and indicates the end of  
 145 dynamic softness (the isotropic rubber modulus increases on heating). (b) The corresponding  
 146 Master Curve of the loss factor  $\tan\delta$  for LCE10, with the frequency scaled for the same  
 147 reference  $T=20^\circ\text{C}$ . Unlike the storage modulus  $E'$ , whose magnitude at high temperatures is  
 148 affected by the nematic-isotropic phase transition and the entropic rubber elasticity, the time-  
 149 temperature superposition for the loss factor works well at this high-temperature / low  
 150 frequency region.

151

152 [Figure 2b](#) shows the same time-temperature superposition for the dynamic loss factor  $\tan\delta$ ,  
153 obtained by scaling the frequency of the tests carried out at different temperatures (as labelled  
154 in the plot, in the same format as in [Fig. 2a](#)). Here, unlike for the storage modulus in [Fig.2a](#), the  
155 frequency scaling works well for high temperatures, producing the predicted values at ultra-low  
156 frequencies (for the reference temperature of 20°C). The frequency band where LCE materials  
157 show high damping is roughly between 0.1 Hz and 20 kHz at ambient temperature. As usual in  
158 time-temperature superposition, this window proportionally shifts to higher frequencies for a  
159 higher reference temperature, and vice-versa for a lower reference temperature. However, one  
160 should be careful with interpretation, since the nematic-isotropic phase transformation occurs  
161 around  $T_{NI}=60^{\circ}\text{C}$  in these LCE materials: if the actual LCE is tested above 70°C, it will be plain  
162 isotropic and its vibration damping will not be different from ordinary elastomers irrespective  
163 of the testing frequency. This is because the WLF time-temperature superposition is based on  
164 the (empirically validated) assumption that the internal dynamics are controlled by the ‘cage  
165 confinement’ in the glass state, which gradually gets weaker and eventually gets fully released  
166 in the melt state. In the nematic LCE, the internal dynamics are slowed down by the  
167 orientational relaxation modes, but only at a temperature within the thermodynamic nematic  
168 phase: unlike glass, a different thermodynamic phase cannot be produced by changing the input  
169 frequency of probing oscillation.

170

### 171 Testing of impact damping

172 The impact damping was tested in the Hopkinson split pressure bar experiment and also in a  
173 separate but closely related ball-impact test. The Hopkinson bar test is based on the impact of  
174 two parallel faces of metal bars, with the test sample inserted in the impact area; it is well  
175 described in the ASM Handbook volume.<sup>22</sup> However, we quickly established that inserting a  
176 flat elastomeric pad in such an impact only activates the compressional deformation modes, and  
177 therefore shows no significant effect of the LCE dynamic softness: the test probes the bulk

178 modulus, which is approximately the same in all elastomers (see [Supplementary](#) for further  
179 detail and plotted data). LCE10, LCE40, as well as ordinary siloxane and thermoplastic  
180 polyurethane elastomers from the market-leading vibration damping suppliers Sylgard® and  
181 Sorbothane®, respectively, all showed the same effect of dissipating about 25-27% of impact  
182 energy in this geometry.

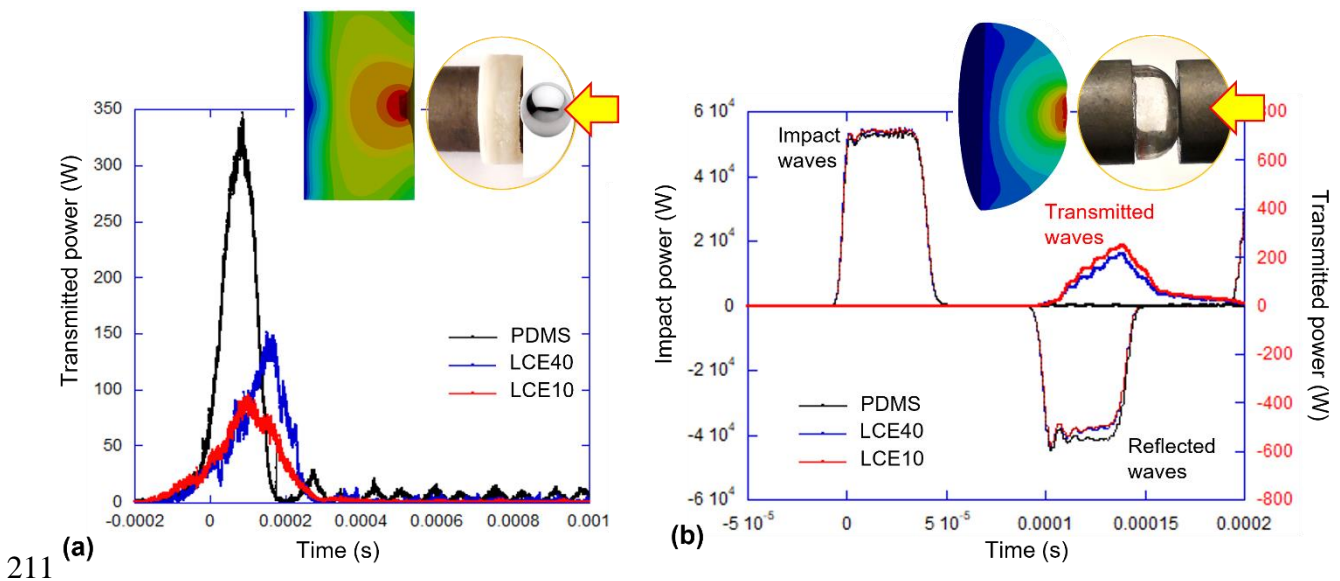
183

184 For this reason, we looked into exploring the impact geometry where the shear deformation  
185 modes are excited, the most straightforward being the impact of a flat elastomeric pad with a  
186 spherical projectile ball, which initially produces spherical waves from the point of impact. This  
187 was tested in two settings: [Figure 3a](#) shows the results of impacting a flat elastomer pad with a  
188 spherical projectile, while [Fig. 3b](#) presents the impact of the flat face of the Hopkinson split  
189 pressure bar on a semi-spherical cap of the elastomer. In both cases, a significant shear  
190 deformation component is generated in the material, and the comparison between the ordinary  
191 elastomers and LCE is stark. Integrating the measured power over time allows us to estimate  
192 the full energy budget: the initial kinetic energy converting into the transmitted, reflected, and  
193 dissipated “lost” energy. For example, for the spherical projectile impact on an elastomer pad  
194 of 3mm thick, with the initial energy of 3J, we found that the PDMS had 25% of energy in the  
195 rebound, 1.2% of energy transmitted, with ca. 74% of impact energy dissipated. For the same  
196 3mm-thick LCE40 pad the results showed 6% of energy in the rebound, 0.7% of energy  
197 transmitted, with ca. 93% of impact energy dissipated, and for LCE10: 5% of energy in the  
198 rebound, 0.6% of energy transmitted, with ca. 94% of impact energy dissipated.

199

200 In the impact of the flat face of split Hopkinson bar on a semi-spherical cap of an elastomer, of  
201 10mm diameter ([Fig. 3b](#)), receiving a strike with the impact energy of 2J, we found that the  
202 PDMS cap had almost no energy transmitted, but rebounded 79% of impact energy (with 21%  
203 energy loss). The LCE damping caps did transmit a very small fraction of impact energy:

204 LCE40 transmitted 0.3%, rebound 72% (loss 27.5%), and LCE10 transmitted 0.4%, rebound  
 205 71% (loss 28.5% of impact energy). It is clear that the shape and dimensions of the damping  
 206 pad play a significant role in this energy distribution. However, we note that even with  
 207 spherical-cap shaped pads, the mechanical loss in the material was comparable between PDMS  
 208 and LCE systems, and much lower than in the projectile-impact test (where very little energy  
 209 was in the rebound). In both tests, the PDMS elastomer had a distinct elastic response with  
 210 resonance bounces, in contrast to both LCE materials showing a strongly overdamped response.



212 **Fig. 3. Impact damping test.** (a) Spherical ball impact on a flat elastomer pad. The incident  
 213 kinetic energy of ca. 3J was partially transmitted through the elastomer into the receiving bar,  
 214 the plot showing the power transmitted after the impact at  $t=0$ s. PDMS sample has 74% of  
 215 impact energy dissipated, and clearly shows the under-damped oscillations after impact. Both  
 216 LCE samples have dissipated over 90% of impact energy, and show the overdamped response  
 217 both at the onset and after the force pulse. (b) Flat surface impact on a semi-spherical elastomer  
 218 pad (of PDMS, LCE40 and LCE10), showing the low and heavily overdamped wave  
 219 transmission: of the impact energy of 2J, only 0.01J (0.4%) was transmitted into the target rod  
 220 by the LCEs while almost all energy was reflected by PDMS, with 28% of impact energy  
 221 absorbed in the elastomers in this geometry. In both panels, the sketches illustrate the geometry  
 222 of impact and the deformation field distribution in the elastomer.

223

224 It is important to establish a correspondence between the impact measurements,  
225 providing data in real time, and the frequency domain where we see both the material properties  
226 (such as Master Curves in Fig. 2) and the elastic waves. For this, we examined the spectral  
227 distribution of power transmission in the ball impact, Fig. 3(a), also see Supplementary Fig. S3.  
228 As expected for the sharp, 0.2 ms pulse in real time, its frequency distribution is a relatively  
229 flat-top until the cutoff frequency for PDMA at ca. 8 kHz, and ca. 10 kHz for both LCE40 and  
230 LCE10. This frequency range captures almost all of the enhanced- $\tan\delta$  region in the Master  
231 Curve in Fig. 2(b), which explains the almost complete dissipation of the impact energy in the  
232 material.

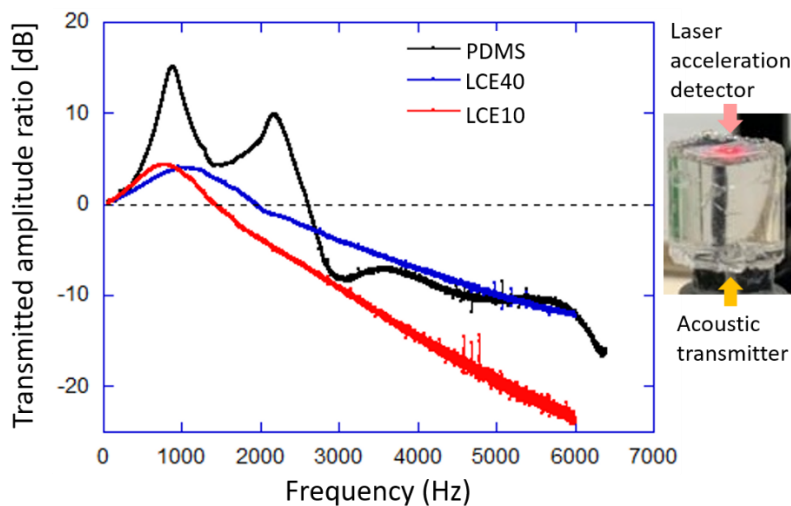
233

#### 234 Testing of vibration attenuation

235 The study of transmission and attenuation of vibrations, particularly in the sonic range from 50  
236 Hz to 6000 Hz, were carried out on a home-made device, described in Supplementary Fig. S6.  
237 To generate spherical waves,<sup>23</sup> and thus explore their shear deformation component, the  
238 cylindrical elastomer sample was held upright; this way, the elastic waves were initially  
239 radiating spherically before the resonant standing wave pattern was established in the  
240 cylindrical samples. Three sets of cylindrical samples were prepared with a similar length of  
241 15-16 mm and a cross-sectional diameter of 17 mm (by crosslinking in the mold). Two samples  
242 were LCE 10 and LCE 40, and one sample was PDMS, used mainly for comparison and  
243 benchmarking. Each sample was mounted on a dynamic shaker that sends elastic waves  
244 longitudinally through the bottom surface of the sample, as illustrated in Figure 4. A dynamic  
245 laser interferometer was used to pick up the acceleration at the top surface (the output signal  
246 from the structure), and an accelerometer was used to measure the acceleration at the bottom  
247 surface (the input signal to the structure).

248

249 **Figure 4** shows the damped-oscillator wave resonance of the system, again comparing LCE  
 250 materials with the standard PDMS elastomer. The results show resonances of the three samples  
 251 at around 1000 Hz (see **Supplementary Fig. S7** for detailed modal analyses). The resonance of  
 252 the PDMS has a peak value of 15 dB. In reference to the PDMS resonance peak, the LCE  
 253 samples showed a much lower peak response which was around 4.5 dB. These peak values of  
 254 the LCE samples are more than two times less than that of the PDMS sample for similar size,  
 255 form and vibration mode. This suggests the existence of higher damping values in the LCE  
 256 samples in comparison to the PDMS.



257  
 258 **Fig. 4. Vibration attenuation test.** The amplitude of the signal (measured in [dB] as a ratio to  
 259 the incident amplitude) transmitted through the elastomer cylinder is plotted against the  
 260 vibration frequency. The primary standing wave resonance near 1 kHz is found in all materials,  
 261 with underdamped PDMS showing several secondary resonance peaks. The overdamped LCE  
 262 systems have the Q-factor equal to 0.4 (i.e. the damping ratio  $\zeta=120\%$ ), compared with PDMS:  
 263  $Q=2.4$  ( $\zeta=21\%$ ). Supplementary Figure S4 shows graphical representations of resonance modes.  
 264

265 In comparison to the results in the impact case shown earlier, a wide-area transducer generating  
 266 longitudinal compression waves shows no effect of the LCE dynamic softness. In the impact  
 267 case, the waves of compressional deformation propagate and attenuate similarly to all  
 268 elastomers. We measured the speed of longitudinal elastic wave travelling along the cylinder

269 length (ca. 15mm), as  $c=49$  m/s for PDMS, 43 m/s for LCE10, and 62 m/s for LCE40. Given  
270 that the density of all elastomers is similar, ca.  $1200 \text{ kg/m}^3$ , these values confirm that it is the  
271 shear (rubber) modulus that is responsible for the acoustic wave: the typical values of rubber  
272 modulus are  $G=1-2$  MPa (for the modulus at a given frequency one should consult the Master  
273 Curve in Fig.2a), which closely matches the measured wave speed  $c \approx \sqrt{G/\rho}$  (the precise  
274 value of wave speed is affected by many additional factors: from the sample shape to the elastic  
275 impedance). It is also consistent that LCE10 and PDMS had approximately the same  
276 crosslinking density (hence a similar rubber modulus), and therefore a comparable wave speed,  
277 while LCE40 had a higher crosslinking density, and accordingly, a slightly higher wave speed.  
278 For comparison, the bulk modulus of all elastomers is approximately the same,  $K=1-2$  GPa,  
279 predicting a typical speed of longitudinal compression wave in the order of 1000 m/s: such a  
280 fast wave zips across the 15mm distance in ca. 15  $\mu\text{sec}$ , and therefore would affect the  
281 measurement above 60 kHz, well outside our testing range.

282

283 The attenuation of the acoustic waves in the elastomers was measured via the damping of the  
284 primary resonance peak, which was found around 1 kHz in all materials, consistently with the  
285 separately measured wave speed and the distance to travel. The quality factor  $Q$  of the resonance,  
286 defined as the frequency-to-bandwidth ratio of the resonator is calculated using the -3dB  
287 method<sup>24</sup>), was determined as  $Q=2.4$  for PDMS (the damping ratio  $\zeta=21\%$ , indicating the  
288 underdamped material). This is consistent with several secondary resonances seen in the PDMS  
289 transmission data in Fig. 4 and also with the secondary vibrations in the impact test seen in Fig.  
290 3a. In contrast, the LCE materials are heavily overdamped:  $Q=0.42$  ( $\zeta=120\%$  for LCE40, and  
291  $Q=0.45$  ( $\zeta=110\%$ ) for LCE10. The difference between LCE10 and LCE40 is within the  
292 uncertainty of the test, influenced by precise details of the surface cut, the cylinder width and  
293 length, and even the placement of the transducer. It is consistent with the theoretical

294 understanding that the anomalous vibration dissipation, on the microscopic level, is caused by  
295 the local rotations of the nematic director, which occur on the length scale well below the  
296 network mesh size given by crosslinking density (an extensive discussion of this theory can be  
297 found in refs. <sup>4,11,12</sup>).

298

## 299 **Discussion**

300 There are three aspects that we touch on in this paper: the choice of LCE material for optimised  
301 mechanical damping, the effect of the sample shape, and the comparison of damping tests done  
302 in the time domain (impact damping) and in the frequency domain (acoustic attenuation). The  
303 early damping studies were conducted on side-chain LCE,<sup>16</sup> and have demonstrated a higher  
304 loss factor  $\tan\delta$  than we see in [Fig.2b](#). However, the mechanical strength and ductility of side-  
305 chain LCE are notoriously low, and we have instead chosen to work with the new generation  
306 of main-chain thiol-acrylate LCE,<sup>20</sup> on which there have already been a number of recent  
307 investigations.<sup>25,26</sup> Although the loss factor seldom exceeds 0.8 in these materials, the  
308 mechanical strength and durability make them a good choice for many application settings. We  
309 have discussed in the text, and quoted the literature on elastic wave theory, to highlight the fact  
310 that to reach the desired regime of dynamic softness (and with it, the enhanced damping), one  
311 must ensure that shear deformation occurs in the material. The geometries that are sustained by  
312 compressional deformations are controlled by the high bulk modulus of elastomers and make a  
313 little damping effect. To achieve these shear deformations, we elected to generate spherical  
314 waves: radiating from an impact point of projectile or emitted by a small transducer, or reflected  
315 from a spherical sample boundary. Note that in the latter case, the amount of dissipated energy  
316 was much lower than when genuine spherical waves were generated (see the discussion of  
317 [Fig.3b](#)).

318

319 Our main focus was on comparing and contrasting the two testing approaches: the impact study,  
320 which explores the process in real time, and the study of elastic wave propagation that looks  
321 for frequency-dependent transmission and resonances. The narrow pulse of impact is a sum of  
322 many frequencies, but even though we did examine its spectral distribution ([Supplementary Fig.  
323 S5](#)) is not easy to quantitatively relate the two techniques due to the different excited ranges  
324 and also the finite size and shape of the samples in both measurements. Two important  
325 correlations reassure us that they both return compatible results. The underdamped elastic  
326 response of PDMS shows in different ways in the two tests, but is clear and unambiguous – as  
327 is the heavily overdamped nature of LCE materials. The ‘slowing down’ of the response to  
328 impact means that the acceleration that the projectile experiences is lower (since the time of the  
329 impact going in and back out is longer). This has an important implication for the use of LCE  
330 as protective layer, because it is the acceleration of the impactor that determines its fate (see,  
331 for instance, the ASTM F2656 standard test method for crash testing of vehicles). Turning to  
332 the other side of the protective pad, we highlight the low amount of energy transmitted through  
333 even a thin pad into the target. We are not sure why there was no registered transmission in the  
334 case of a semi-spherical PDMS cap with a flat-face strike, but we suspect it was a fortuitous  
335 accident of internal resonance in the elastic medium, which resulted in the full rebound.  
336 Looking at all the results, it is clear that the impact transmission through the LCE protective  
337 pad is consistently very low, which invites a different set of applications (when the stationary  
338 object behind the pad is protected).

339

340 Our aim was to present and compare the two testing methods, impact and acoustic, and bring  
341 them closer to some standard that could be consistently applied in different applications and  
342 materials, as well as summarise the LCE characterization via Master Curves. For advanced  
343 applications, this field will clearly develop into using composites, generating complex shear-  
344 rich local deformations in the matrix, with highly-damping LCE dispersed in elastic structures:

345 this is already an approach pursued in the recent literature.<sup>13,24</sup> The research field will extend  
346 towards including LCE materials within layered and latticed composite structures, resulting in  
347 constrained damping layer technologies of superior performance. Furthermore, LCEs have  
348 excellent properties for inclusion within low-frequency damping and sonic sealing applications.  
349

## 350 **Methods**

351 **Materials and preparation of LCE.** For the preparation of LCE, we followed the methods  
352 reported previously, with a single-step crosslinking reaction of thiol-acrylate Michael  
353 addition.<sup>27</sup> The diacrylate monomer, 1,4-bis-[4-(3-acryloyloxypropyloxy) benzoyloxy]-  
354 2-methylbenzene (RM257) was purchased from Daken Chemical Co. The dithiol spacer, 2,2'-  
355 (ethylenedioxy) diethanethiol (EDDET), and tetrathiol crosslinker pentaerythritol tetrakis (3-  
356 mercaptopropionate) (PETMP), were purchased from Sigma Aldrich. Triethylamine (TEA,  
357 Sigma Aldrich) was used as the catalyst of the thiol-acrylate Michael-addition reaction. As the  
358 radical scavenger, butylated hydroxytoluene (BHT, from Sigma Aldrich) was used to suppress  
359 the unwanted radical polymerisation reaction between acrylates. All chemicals were used in  
360 their as-received condition with no purification.

361 At the specific molar ratio of functional groups shown in [Supplementary Table S1](#), RM257,  
362 EDDET, PETMP and BHT (0.5wt%) were weighed. After each mixture was gently mixed at  
363 an elevated  $T \sim 90^\circ\text{C}$  for  $\sim 10$  min, TEA was added at 0.8wt% to start the Michael-addition  
364 reaction between thiol and acrylate groups. The mixture was then transferred into a Teflon mold  
365 to complete the polymerization at  $90^\circ\text{C}$  (isotropic phase) overnight.

366

367 **Stress-strain response.** The stress-strain curves for LCE films on the tensile mode were  
368 obtained using a home-made tensile testing rig, delivering a controlled deformation rate over a  
369 large range (to cover a large sample extension needed to pick all key regimes of LCE stress

370 response). The measured tensile force was converted into engineering tensile stress by dividing  
371 over the initial sample ratio.

372

373 **Dynamic-mechanical characterization:** The small-amplitude oscillating measurements were  
374 carried out on TA DMA 850 instrument in tensile mode. The constant-frequency temperature  
375 scans were performed to identify the key phases of the materials (glass, nematic, isotropic  
376 rubber). For this, we used the low frequency of 1 Hz to obtain the storage modulus closer to the  
377 expected equilibrium values of the Young modulus in different phases. The elevated values of  
378 the loss factor indicated enhanced mechanical dissipation across the nematic phase.

379 The time-temperature superposition was used to produce dynamic Master Curves of elastomers  
380 at a chosen reference temperature. As is standard in the WLF method, we carried out frequency  
381 scans in the available range of 0.01–200 Hz at different temperatures, and then scaled the  
382 frequency by a temperature-dependent factor  $\alpha(T)$  to achieve the overlapping of consecutive  
383 scans. This was successful across the glass transition (for which the WLF method is designed);  
384 however, crossing the nematic-isotropic transition makes it impossible to overlap the modulus  
385 curves since the overall modulus magnitude changes (downwards) due to the nematic softness  
386 and (upwards) due to the entropic rubber-elastic effect on heating. We left the high-temperature  
387 data un-scaled across the nematic transition for the  $E'(\omega)$  Master Curves. In contrast, the  
388 superposition of the loss factor worked perfectly across the nematic-isotropic transition.

389 **Split Hopkinson bar experiment:** The classical home-made setup involves two identical bars  
390 (using soft magnesium to improve the impedance ratio between the metal and the elastomer),  
391 with the sample fixed on the front face of the “transmitted bar”, waiting to be struck by the  
392 “incident bar”, which is accelerated by the controlled pneumatic striker. The sequence of  
393 piezoelectric strain gauges is fixed on both bars to register the longitudinal elastic wave  
394 travelling along each of them. The overall energy balance of initial and reflected elastic wave

395 energy in the incident bar, plus the wave energy in the transmitted bar, allows us to accurately  
396 find the amount of energy dissipated in the elastomer.

397 In a modification of this test, we have replaced the incident bar with an air gun firing a steel  
398 ball projectile, with a sequence of LVDT sensors registering its speed as the ball passes along  
399 the barrel initially, and after reflection. The strain gauge in the transmitted bar provides the data  
400 on transmitted force and velocity, which can be converted into the transmitted power. The  
401 overall energy balance of initial and reflected kinetic energy of the projectile, plus the  
402 mechanical energy transmitted into the bar, allows to find the dissipated energy.

403 **Elastic wave attenuation experiment:** The acoustic attenuation was studied on a home-made  
404 laser vibrometer setup. A dynamic shaker (Modal Shop K2007E01) was used to generate a  
405 periodic chirp signal, generating a surface acceleration ranging between 0.2 and 0.6 m/s<sup>2</sup>. The  
406 dynamic force at the input surface of the structure was measured using an impedance head (PCB  
407 288D01) with a sensitivity of 22.4 mV/N. The internal resonance of the setup comprising the  
408 impedance head and dynamic shaker occurred at 7500 Hz; thus our measurement was restricted  
409 to below 6000 Hz. The acceleration at the output surface of the structure was measured by a  
410 laser vibrometer system (Polytec PDV-100), mounted vertically above the flat cylinder surface.  
411 The ratio of output-to-input amplitude was converted to dB for presentation.

#### 412 **Acknowledgements**

413 This work was supported by the European Research Council H2020 via the Advanced Grant  
414 No: 786659 (E.M.T.) and the CleanSky SilentProp Grant No: 882842 (D.C.). The authors are  
415 grateful for many useful communications and help from A. Gablier and Herman Guo.

#### 416 **Author contributions**

417 M.O.S., A.T. and E.M.T. conceived the central idea. M.O.S. designed the LCEs. W.E., D.C.  
418 and D.W. performed the main experiments. All authors contributed to the data analysis,  
419 interpretation, and writing the manuscript.

420

421 **Competing interests**

422 The authors declare no competing interests.

423

424 **References**

---

- <sup>1</sup> A. D. Nashif, D. I. G. Jones, J. P. Henderson, *Vibration Damping* (Wiley, New York, 1985).
- <sup>2</sup> G. R. Tomlinson, 3rd International Conference on Intelligent Materials, ISBN 0-8194-2165-0, 1996, p. 656.
- <sup>3</sup> J. D. Ferry, *Viscoelastic Properties of Polymers*, 3rd ed. (Wiley, New York, 1980).
- <sup>4</sup> N. G. McCrum, B. E. Read, and G. Williams, *Anelastic and Dielectric Effects in Polymer Systems* (Dover, New York, 1967).
- <sup>5</sup> M. Warner, and E. M. Terentjev, *Liquid Crystal Elastomers* (Oxford Univ. Press, Oxford, 2007).
- <sup>6</sup> N. A. Fleck and J. W. Hutchinson, *Adv. Appl. Mech.* 33, 295 (1997).
- <sup>7</sup> K. Bhattacharya, G. Friesecke, and R. D. James, *Proc. Natl. Acad. Sci. U.S.A.* 96, 8332 (1999).
- <sup>8</sup> M. Warner, P. Bladon, and E. M. Terentjev, *J. Phys. II* 4, 93 (1994).
- <sup>9</sup> S. M. Clarke, E. M. Terentjev, I. Kundler, and H. Finkelmann, *Macromolecules* 31, 4862 (1998).
- <sup>10</sup> K. Urayama, R. Mashita, I. Kobayashi, and T. Takigawa, *Macromolecules* 40, 7665 (2007).
- <sup>11</sup> A. Hotta and E. M. Terentjev, *Eur. Phys. J. E* 10, 291 (2003).
- <sup>12</sup> E. M. Terentjev, A. Hotta, S. M. Clarke, and M. Warner, *Phil. Trans. R. Soc. Lond. A* 361, 653 (2003).
- <sup>13</sup> D. R. Merkel, R. K. Shaha, C. M. Yakacki and C. P. Frick, *Polymer*, 166, 148 (2019).
- <sup>14</sup> T. Ohzono, M. O. Saed, E. M. Terentjev, *Adv. Mater.* 31, 1902642 (2019).
- <sup>15</sup> L. J. Fradkin, I. V. Kamotski, E. M. Terentjev, and D. D. Zakharov, *Proc. R. Soc. Lond. A* 459, 2627 (2003).
- <sup>16</sup> S. M. Clarke, A. R. Tajbakhsh, E. M. Terentjev, C. Remillat, G. R. Tomlinson, J. R. House, *J. Appl. Phys.* 89, 6530 (2001).
- <sup>17</sup> T. C. Lubensky, E. M. Terentjev, and M. Warner, *J. Phys. II* 4, 1457 (1994).
- <sup>18</sup> I. A. Rousseau, and P. T. Mather, *J. Am. Chem. Soc.* 125, 15300 (2003).
- <sup>19</sup> H. P. Patil, D. M. Lentz, and R. C. Hedden, *Macromolecules* 42, 3525 (2009).
- <sup>20</sup> C. M. Yakacki, M. Saed, D. P. Nair, T. Gong, S. M. Reed, C. N. Bowman, *RSC Adv.* 5, 18997 (2015).
- <sup>21</sup> S. V. Fridrikh and E. M. Terentjev, *Phys. Rev. E* 60, 1847 (1999).
- <sup>22</sup> G. T. Gray III and W. R. Blumenthal, *Split Hopkinson pressure bar testing in soft materials*. In: ASM Handbook, vol.8: Mechanical Testing and Evaluation (ed. H. Kuhn and D. Medlin, ASM International, 2000)
- <sup>23</sup> L. J. Fradkin, A. P. Kiselev, *J. Acoust. Soc. Amer.* 101, 52 (1997).
- <sup>24</sup> C. W. Bert, *J. Sound Vib.* 29, 129 (1973).
- <sup>25</sup> C. Luo, C. Chung, N. A. Traugutt, C. M. Yakacki, K. N. Long, K. Yu, *ACS Appl. Mater. Interfaces* 13, 12698–12708 (2021).
- <sup>26</sup> N. A. Traugutt, D. Mistry, C. Luo, K. Yu, Q. Ge, C. M. Yakacki, *Adv. Mater.* 32, 2000797 (2020).
- <sup>27</sup> M. O. Saed, A. H. Torbati, C. A. Starr, R. Visvanathan, N. A. Clark, C. M. Yakacki, *J. Polym. Sci. Part B: Polym. Phys.* 55, 157-168 (2017).